PROJECTION-FREE APPROXIMATION OF FLOWS OF HARMONIC MAPS WITH QUADRATIC CONSTRAINT ACCURACY AND VARIABLE STEP SIZES

GEORGIOS AKRIVIS, SÖREN BARTELS, MICHELE RUGGERI, AND JILU WANG

Abstract. We construct and analyze a projection-free linearly implicit method for the approximation of flows of harmonic maps into spheres. The proposed method is unconditionally energy stable and, under a sharp discrete regularity condition, achieves second-order accuracy with respect to the constraint violation. Furthermore, the method accommodates variable step sizes to speed up the convergence to stationary points and to improve the accuracy of the numerical solutions near singularities, without affecting the unconditional energy stability and the constraint violation property. We illustrate the accuracy in approximating the unit-length constraint and the performance of the method through a series of numerical experiments, and compare it with the linearly implicit Euler and two-step BDF methods.

1. Introduction

Let $\Omega \subset \mathbb{R}^d$ denote a bounded domain with Lipschitz boundary $\partial\Omega$, and let $\Gamma_{\mathrm{D}} \subset \partial\Omega$ be the Dirichlet part of the boundary, of positive surface measure. Harmonic maps (into the sphere) are the stationary points of the Dirichlet energy functional

$$I[u] = \frac{1}{2}\int_\Omega |\nabla u|^2 \,\mathrm{d}x,$$

among all vector fields $u \in H^1(\Omega;\mathbb{R}^\ell)$ satisfying the unit-length constraint $|u| = 1$ a.e. in Ω, subject to Dirichlet boundary conditions $u|_{\Gamma_{\mathrm{D}}} = u_{\mathrm{D}}$. Here, $H^1(\Omega;\mathbb{R}^\ell)$ denotes the Sobolev space consisting of vector fields $u : \Omega \to \mathbb{R}^\ell$ in $L^2(\Omega;\mathbb{R}^\ell)$ with square-integrable gradients, while $u_{\mathrm{D}} : \Gamma_{\mathrm{D}} \to \mathbb{R}^\ell$ is a given function, which is assumed to be equal to the trace of a function $\tilde{u}_{\mathrm{D}} \in H^1(\Omega;\mathbb{R}^\ell)$ with $|\tilde{u}_{\mathrm{D}}| = 1$ a.e. in Ω. The resulting Euler–Lagrange equations are

$$\begin{aligned} &-\Delta u = \lambda u, \qquad |u| = 1 \ \text{ in } \Omega, \\ &u = u_{\mathrm{D}} \ \text{ on } \Gamma_{\mathrm{D}}, \quad \frac{\partial u}{\partial n} = 0 \ \text{ on } \partial\Omega \setminus \Gamma_{\mathrm{D}}. \end{aligned} \tag{1}$$

The function $\lambda = |\nabla u|^2$ is the Lagrange multiplier related to the unit-length constraint; see [12, Ch. 7] and references therein.

Date: February 11, 2026.

2020 *Mathematics Subject Classification.* 35J50, 35J62, 35K59, 65M15, 65M60.

Key words and phrases. harmonic map, gradient flow, midpoint method, unit-length constraint.

Acknowledgments. The first author gratefully acknowledges the support and warm hospitality of the Harbin Institute of Technology, Shenzhen, China. The second author gratefully acknowledges financial support by the German Research Foundation (DFG) via the Research Unit FOR 3013 *Vector- and tensor-valued surface PDEs* (Project No. 417223351). The work of the third author was partially supported by the Istituto Nazionale di Alta Matematica (INdAM) (research project GNCS 2024 – CUP E53C23001670001). The work of the fourth author was partially supported by the National Natural Science Foundation of China (Project No. 12471371).

Gradient flows provide an attractive tool to solve the Euler–Lagrange equations as these decrease the Dirichlet energy along trajectories. The simplest case corresponds to the L^2-gradient flow and it is known as the harmonic map heat flow (into spheres)

$$\partial_t u - \Delta u = |\nabla u|^2 u, \quad |u|^2 = 1 \ \text{ in } \Omega, \tag{2}$$

subject to initial and boundary conditions $u(0,\cdot) = u^0 \in \mathcal{A}_{u_\mathrm{D}}$ and $u(t,\cdot)|_{\Gamma_\mathrm{D}} = u_\mathrm{D}$, where the class of admissible vector fields $\mathcal{A}_{u_\mathrm{D}}$ is defined by $\mathcal{A}_{u_\mathrm{D}} := \{u \in H^1(\Omega;\mathbb{S}^{\ell-1}) : \ u|_{\Gamma_\mathrm{D}} = u_\mathrm{D}\}$ and $\mathbb{S}^{\ell-1} := \{v \in \mathbb{R}^\ell : |v| = 1\}$ denotes the unit sphere in $\mathbb{R}^\ell$. Under our assumptions, $\tilde{u}_\mathrm{D} \in \mathcal{A}_{u_\mathrm{D}}$; in particular, $\mathcal{A}_{u_\mathrm{D}} \neq \emptyset$.

Equation (2) and various generalizations appear in numerous applications, including the Landau–Lifshitz–Gilbert (LLG) equation for magnetization dynamics [8], models of nematic liquid crystals [18], and geometric evolution equations describing mean curvature flow of surfaces [25, 26]. A common feature in these applications is that the exact solution inherently satisfies a unit-length constraint. This intrinsic requirement has inspired the development of efficient numerical methods that preserve the unit-length property at the discrete level.

One straightforward approach involves the renormalization of numerical solutions using post-processing techniques to restore the crucial unit-length attribute to the solutions. Numerical methods that incorporate a projection step to satisfy the constraint at certain nodes exactly lead to restrictions concerning the step size or the class of admissible triangulations; see [11, 10, 6, 7]. Newton schemes can in general only be guaranteed to converge locally in the neighborhood of a sufficiently regular energy-stable solution [17]. Methods that satisfy the constraint everywhere make use of appropriate nonlinear interpolation procedures and are known to be optimally convergent for certain sufficiently regular solutions; see [22]. The optimal convergence of piecewise affine finite element discretizations with nodal constraints has been established in [24, 17]. An alternative approach to develop higher-order schemes for the harmonic map heat flow and the LLG equation can be based on equivalent unconstrained formulations; cf. [16]. This however requires the solution of nonlinear systems of equations in each time step.

The standard variational formulation of the Euler–Lagrange equations (1) is to seek a vector field $u \in \mathcal{A}_{u_\mathrm{D}}$ such that

$$(\nabla u, \nabla v) = \int_\Omega |\nabla u|^2 u \cdot v \,\mathrm{d}x \tag{3}$$

for all $v \in H^1_\mathrm{D}(\Omega;\mathbb{R}^\ell) \cap L^\infty(\Omega;\mathbb{R}^\ell)$; the test space in (3) is dictated by the fact that $|\nabla u|^2 u \in L^1(\Omega;\mathbb{R}^\ell)$. Here, $H^1_\mathrm{D}(\Omega;\mathbb{R}^\ell)$ denotes the subspace of $H^1(\Omega;\mathbb{R}^\ell)$ made of all functions with vanishing traces on Γ_D. An alternative formulation, due to Alouges [5], is

$$(\nabla u, \nabla v) = 0 \tag{4}$$

for all $v \in T_u$, where

$$T_u := \{v \in H^1_\mathrm{D}(\Omega;\mathbb{R}^\ell) : v \cdot u = 0 \text{ a.e. in } \Omega\}$$

represents a solution-dependent test space, a closed subspace of $H^1_\mathrm{D}(\Omega;\mathbb{R}^\ell)$; see, e.g., [12, Ch. 7] for further details. The alternative form (4) appears much simpler. Even though the test space T_u depends on the solution u, the primary advantage of (4) is that it can be easily linearized; see [5]. Based on formulation (4), several projection-free linear schemes are proposed in [13]; the resulting constraint violation is controlled linearly by the step size, independently of the number of iterations. The approach has then been used for various related problems in [1, 23, 28].

We now describe the main idea of the projection-free linearly implicit Euler scheme. In [13], semi-implicit time discretization schemes are introduced for gradient flow problems represented by

$$(u_t, v)_\star + (\nabla u, \nabla v) = 0, \tag{5}$$

subject to initial and boundary conditions $u(\cdot,0) = u^0 \in \mathcal{A}_{u_\mathrm{D}}$ and $u(\cdot,t)|_{\Gamma_\mathrm{D}} = u_\mathrm{D}$. The variational formulation (5) holds for a.e. $t \in [0,T]$ for some final time $T > 0$, and for all test functions $v \in T_{u(t)}$. The pointwise unit-length constraint is imposed in the equivalent form $u_t \cdot u = 0$. The inner product $(\cdot,\cdot)_\star$ can be either the L^2- or the H^1-inner product, denoted by $(\cdot,\cdot)$ and $(\nabla\cdot,\nabla\cdot)$, respectively. Equation (5) then represents either the L^2- or the H^1-gradient flow for harmonic maps into spheres, respectively.

Starting from u^0, the projection-free linearly implicit Euler method iteratively computes a sequence $(u^n)_{n\geqslant 1}$ of approximations as follows: For a fixed step size τ, let $d_t u^n := (u^n - u^{n-1})/\tau$ denote the backward difference quotient. At each iteration, one seeks $d_t u^n \in H^1_\mathrm{D}(\Omega;\mathbb{R}^\ell)$, satisfying the discrete linearized unit-length condition $d_t u^n \cdot u^{n-1} = 0$, such that

$$(d_t u^n, v)_\star + (\nabla u^{n-1} + \tau \nabla d_t u^n, \nabla v) = 0 \tag{6}$$

for all $v \in H^1_\mathrm{D}(\Omega;\mathbb{R}^\ell)$ with $v \cdot u^{n-1} = 0$. The new approximation is then given by $u^n := u^{n-1} + \tau d_t u^n$ and satisfies the required Dirichlet boundary condition $u^n|_{\Gamma_\mathrm{D}} = u_\mathrm{D}$. Note that (6) can be reformulated as

$$(d_t u^n, v)_\star + (\nabla u^n, \nabla v) = 0 \tag{7}$$

for all $v \in H^1_\mathrm{D}(\Omega;\mathbb{R}^\ell)$ with $v \cdot u^{n-1} = 0$. The iteration is unconditionally well posed and energy decreasing; indeed, choosing $v = \tau\, d_t u^n$ in (7) yields

$$\frac{1}{2}\|\nabla u^n\|^2 - \frac{1}{2}\|\nabla u^{n-1}\|^2 + \tau\|d_t u^n\|_\star^2 + \frac{\tau^2}{2}\|\nabla d_t u^n\|^2 = 0, \tag{8}$$

which implies, for every $m \geqslant 1$, the energy identity

$$\frac{1}{2}\|\nabla u^m\|^2 + \tau\sum_{n=1}^{m}\|d_t u^n\|_\star^2 + \frac{\tau^2}{2}\sum_{n=1}^{m}\|\nabla d_t u^n\|^2 = \frac{1}{2}\|\nabla u^0\|^2. \tag{9}$$

This yields the summability of the discrete time derivatives $\|d_t u^n\|_\star^2$ and hence the weak convergence of subsequences to solutions of (4). A bound for the constraint violation thus follows from the orthogonality condition and $|u^0| = 1$, as we have

$$|u^m|^2 - 1 = |u^{m-1}|^2 - 1 + \tau^2|d_t u^m|^2 = \cdots = \tau^2\sum_{n=1}^{m}|d_t u^n|^2. \tag{10}$$

By taking the L^1-norm of this identity, the sum on the right-hand side is bounded by $\tau(c_\star/2)\|\nabla u^0\|^2$ provided that the induced norm $\|\cdot\|_\star$ controls the L^2-norm up to a factor $c_\star^{1/2}$ (see (13) below).

The iterative scheme (6) is built upon the weak formulation (5) by Alouges and an implicit Euler temporal discretization. Recently, linearly implicit backward difference formula (BDF) schemes were introduced in [4] for the LLG equation. For the harmonic map heat flow, a numerical approximation employing a nodal treatment of the unit-length constraint was proposed in [15]. More recently, An, Gao, and Sun [9] designed semi-implicit Euler and Crank–Nicolson finite difference projection methods for the LLG equation. A similar semi-implicit approach, but based on the two-step BDF method, was proposed in [20]. These works have yielded optimal/quasi-optimal error estimates, leading to bounds on the constraint violation, in situations involving sufficiently regular solutions.

In this paper, we design a projection-free linearly implicit (θ, μ)-method for flows of harmonic maps, utilizing Alouges' weak formulation, and address its approximation properties when the smoothness of the solution is not guaranteed. Here, $0 < \theta \leqslant 1$ and $0 \leqslant \mu \leqslant 1$ denote two parameters of the method characterizing its energy dissipation and its approach to realize the unit-length constraint, respectively; see Section 2.1 below. The proposed method offers several key advantages: (1) It is unconditionally energy stable and achieves second-order accuracy in approximating the unit-length constraint, requiring only minimal regularity conditions on the solution, akin to the projection-free two-step BDF method proposed in [2]; see Propositions 2.1 and 2.3 below. (2) It accommodates variable step sizes, which paves the way to the application of acceleration techniques for achieving faster convergence to stationary points and adaptive approaches to improve the accuracy of numerical solutions near singularities (such as a singularity at $t = 0$ for nonsmooth initial data or a finite blow-up for smooth initial data), without affecting the unconditional energy stability and the constraint violation property. This capability represents a notable advantage over the projection-free two-step BDF method proposed in [2], as stability for BDF methods in the case of variable step sizes is a delicate matter; see, e.g., [3]. We illustrate the accuracy in approximating the unit-length constraint and the performance of the proposed method through a series of numerical experiments, comparing it with the linearly implicit Euler and two-step BDF methods.

To fix the ideas, we develop our theory for the problem of approximating flows of harmonic maps (into the sphere), which serves as a prototype of a geometrically constrained partial differential equation. Using the same ideas, projection-free linearly implicit iterative schemes with second-order accuracy in the constraint approximation supporting variable step sizes can be designed and analyzed for a broad class of problems, e.g., in micromagnetics, liquid crystal theory, and bending theory. We stress that our results are developed for a semi-discrete method, in which only the time discretization of (5) is considered, but hold verbatim if a spatial discretization with a nodal treatment of the constraint is used; see [13], where a fully discrete method based on first-order finite elements for the linearly implicit Euler method is introduced and analyzed. Moreover, the method can be extended to more general target manifolds than the unit sphere, e.g., to manifolds that can be characterized as the zero level set of a C^2-function satisfying certain growth conditions. Again, we refer to [13], where this extension is developed for the method based on the linearly implicit Euler method.

The paper is organized as follows. In Section 2, we introduce the projection-free linearly implicit (θ, μ)-method and the main theoretical results. For the sake of comparison, we also discuss the implicit Euler method and the two-step BDF method. The extension of the proposed method to accommodate variable step sizes and the corresponding analyses of energy decay and constraint violation are presented in Section 3. Numerical results are provided in Section 4 to support the theoretical analysis and illustrate the performance of the schemes.

In this work, we use standard notation for differential operators and Lebesgue and Sobolev spaces. We let $|\cdot|$ denote the Euclidean length of vectors as well as the Frobenius norm of matrices, and $\|\cdot\|$ the L^2-norm of functions or vector fields.

2. Projection-free methods and main results

In this section, we introduce a projection-free linearly implicit method for the time discretization of flows of harmonic maps, which is proved to be of quadratic constraint accuracy. To evaluate and compare the effectiveness of the proposed scheme, we also discuss the projection-free two-step BDF method recently introduced and analyzed in [2].

2.1. **The linearly implicit (θ, μ)-method.** The implicit Euler method (6) proposed in [13] is known as the simplest projection-free method for harmonic maps, and exhibits only first-order convergence with respect to the step size of the error in the unit-length constraint. In this subsection, we generalize the approach to obtain a linearly implicit (θ, μ)-method.

Let $t_n = n\tau$ for all $n \geqslant 0$, where $\tau > 0$ denotes a fixed step size. For $n \geqslant 1$ and a sequence $(u^n)_{n\geqslant 0}$ in a Hilbert space, we define

$$d_t u^n := \frac{u^n - u^{n-1}}{\tau}, \quad u^{n-1+\theta} := u^{n-1} + \theta\tau d_t u^n, \quad \widehat{u}^{n-1+\mu} := u^{n-1} + \mu\tau d_t u^{n-1},$$

where $0 \leqslant \theta, \mu \leqslant 1$. Here, $u^{n-1+\theta}$ denotes the interpolated value at $t_{n-1+\theta} = t_{n-1} + \theta\tau$ of the linear interpolant based on (t_{n-1}, u^{n-1}) and (t_n, u^n) (serving as an approximation to $u(t_{n-1+\theta})$), while $\widehat{u}^{n-1+\mu}$ denotes the extrapolated value at $t_{n-1+\mu} = t_{n-1} + \mu\tau$ of the linear interpolant based on (t_{n-2}, u^{n-2}) and (t_{n-1}, u^{n-1}) (serving as an approximation to $u(t_{n-1+\mu})$). Note that, even if $\theta = \mu$, $u^{n-1+\theta} \neq \widehat{u}^{n-1+\mu}$ in general.

Since $\widehat{u}^{n-1+\mu}$ relies on two previous approximations for positive μ, for the given initial value u^0, we first determine a second starting approximation u^1 by employing a single step of the linearly implicit Euler method (6). Subsequently, for given approximations u^{n-2} and u^{n-1}, we seek $d_t u^n \in H^1_{\mathrm{D}}(\Omega; \mathbb{R}^\ell)$, satisfying the linearized unit-length condition $d_t u^n \cdot \widehat{u}^{n-1+\mu} = 0$, such that

$$(d_t u^n, v)_\star + (\nabla u^{n-1+\theta}, \nabla v) = (d_t u^n, v)_\star + (\nabla\big[u^{n-1} + \theta\tau d_t u^n\big], \nabla v) = 0 \tag{11}$$

for all $v \in H^1_{\mathrm{D}}(\Omega; \mathbb{R}^\ell)$ with $v \cdot \widehat{u}^{n-1+\mu} = 0$. Thus, upon computing $d_t u^n$, a new approximation is defined as

$$u^n := u^{n-1} + \tau d_t u^n.$$

The new approximation u^n satisfies the required Dirichlet boundary condition $u^n|_{\Gamma_{\mathrm{D}}} = u_{\mathrm{D}}$, provided the approximation u^{n-1} at the previous time level satisfies this condition.

We will demonstrate that, for suitable choices of the parameters θ and μ, the linearly implicit (θ, μ)-method (11) is energy decreasing and, under a sharp regularity condition on the numerical solution, satisfies a constraint violation estimate of second order. We present the main theoretical results in the next subsection.

Remark 2.1 (relevant choices for θ and μ)**.** *We now comment on the choice of the parameters θ and μ in the proposed method. The resulting schemes will be compared with each other numerically in Section 4.*
(i) For $\theta = 1$ and $\mu = 0$, (11) *reduces to the implicit Euler method* (6)*.*
(ii) For $\theta = 1/2$ and $\mu = 1/2$, we get the linearly implicit midpoint method, which will be unconditionally energy stable and will achieve second-order accuracy in approximating the unit-length constraint; see Propositions 2.1 and 2.3 below.
(iii) For $\theta = 1$ and $\mu = 1/2$, we get a modified implicit Euler method. In this case, the variational formulation (11) *to be solved at each iteration is the same as that of the linearly implicit Euler method* (6)*. However, like in the midpoint method for $n \geqslant 2$, the orthogonality constraint is considered with respect to the extrapolated value $\widehat{u}^{n-1/2}$. We will see that the modified linearly implicit Euler method will be characterized by the same energy decay property* (8) *as the standard linearly implicit Euler method, but will have the same quadratic constraint accuracy as the midpoint method; see Propositions 2.1 and 2.3 below.*

We now summarize the proposed (θ, μ)-method (11) in the following algorithm.

Algorithm 2.1 ((θ, μ)-method)**.** *Choose $u^0 \in H^1(\Omega; \mathbb{R}^\ell)$ with $u^0|_{\Gamma_{\mathrm{D}}} = u_{\mathrm{D}}$ and $|u^0| = 1$.*

(0) Compute $d_t u^1 \in H^1_{\mathrm{D}}(\Omega;\mathbb{R}^\ell)$ *such that* $d_t u^1 \cdot u^0 = 0$ *and*

$$(d_t u^1, v)_\star + (\nabla[u^0 + \tau d_t u^1], \nabla v) = 0$$

for all $v \in H^1_{\mathrm{D}}(\Omega;\mathbb{R}^\ell)$ *with* $v \cdot u^0 = 0$*; set* $u^1 = u^0 + \tau d_t u^1$ *and* $n = 2$.
(1) Set $\widehat{u}^{n-1+\mu} := u^{n-1} + \mu\tau \mathrm{d}_t u^{n-1}$. *Compute* $d_t u^n \in H^1_{\mathrm{D}}(\Omega;\mathbb{R}^\ell)$ *such that* $d_t u^n \cdot \widehat{u}^{n-1+\mu} = 0$ *and*

$$(d_t u^n, v)_\star + (\nabla[u^{n-1} + \theta\tau d_t u^n], \nabla v) = 0$$

for all $v \in H^1_{\mathrm{D}}(\Omega;\mathbb{R}^\ell)$ *with* $v \cdot \widehat{u}^{n-1+\mu} = 0$. *Then, set* $u^n = u^{n-1} + \tau d_t u^n$.
(2) Stop if $\|d_t u^n\|_\star + \theta\tau\|\nabla(d_t u^n)\| \leqslant \varepsilon_{\mathrm{stop}}$ *or if* $n\tau \geqslant T$.
(3) Increase $n \to n+1$ *and continue with (1).*

Remark 2.2. *The first stopping criterion used in Algorithm 2.1, i.e., step (2), applies to the case of energy minimization and is chosen in such a way that, if we define the approximate harmonic map generated by the algorithm as* $u_h^{N_{stop}-1}$*, where* N_{stop} *is the smallest integer for which the stopping criterion is met, then the following relationship holds*

$$(\nabla u_h^{N_{stop}-1}, \nabla v) = R(v) \text{ for all admissible } v \quad \text{and} \quad \|R\|_{H^1(\Omega)^\star} \leqslant \varepsilon_{stop}. \tag{12}$$

The aim is to ensure a fair comparison of the methods in numerical experiments: By utilizing the same tolerance for the standard Euler, modified Euler, and midpoint methods, the resulting approximate harmonic maps satisfy the harmonic map equation (4) *with a comparable accuracy (in the sense that the dual norm of the residual can be bounded by the same tolerance). The second criterion applies to the case in which one is interested in approximating the gradient flow dynamics until a certain prescribed final time* $T > 0$.

2.2. **Energy decay and constraint violation for the (θ, μ)-method.** Hereafter, we assume that the norm induced by the inner product $(\cdot,\cdot)_\star$ satisfies

$$\|v\| \leqslant c_\star^{1/2}\|v\|_\star \quad \text{for all } v \in H^1_{\mathrm{D}}(\Omega;\mathbb{R}^\ell). \tag{13}$$

This inequality trivially holds for both the L^2- and H^1-norms.

In the following proposition, we show the unconditional stability of the method.

Proposition 2.1 (energy identity)**.** *The sequence generated by Algorithm 2.1 satisfies, for all* $m \geqslant 2$*, the energy identity*

$$\frac{1}{2}\|\nabla u^m\|^2 + \tau\sum_{n=1}^m \|d_t u^n\|_\star^2 + \frac{\tau^2}{2}\|\nabla d_t u^1\|^2 + \Big(\theta - \frac{1}{2}\Big)\tau^2\sum_{n=2}^m \|\nabla d_t u^n\|^2 = \frac{1}{2}\|\nabla u^0\|^2. \tag{14}$$

Proof. Testing (11) by the admissible test function $v := d_t u^n$, we have

$$\|d_t u^n\|_\star^2 + (\nabla[u^{n-1} + \theta\tau d_t u^n], \nabla d_t u^n) = 0,$$

i.e.,

$$\|d_t u^n\|_\star^2 + (\nabla u^{n-1/2} + (\theta - 1/2)\tau\nabla d_t u^n, \nabla d_t u^n) = 0,$$

and thus

$$\|d_t u^n\|_\star^2 + \frac{1}{2\tau}\big(\|\nabla u^n\|^2 - \|\nabla u^{n-1}\|^2\big) + \Big(\theta - \frac{1}{2}\Big)\tau\|\nabla d_t u^n\|^2 = 0.$$

Multiplying this relation by τ and summing over n from $n = 2$ to $n = m$ yields

$$\frac{1}{2}\|\nabla u^m\|^2 + \tau\sum_{n=2}^m \|d_t u^n\|_\star^2 + \Big(\theta - \frac{1}{2}\Big)\tau^2\sum_{n=2}^m \|\nabla d_t u^n\|^2 = \frac{1}{2}\|\nabla u^1\|^2.$$

Using the energy identity (8) for the first step ($n = 1$) performed with the linearly implicit Euler method, we obtain the asserted identity. □

We now proceed with studying the constraint violation properties, which provide an unconditional linear rate and a quadratic rate under a mild but necessary discrete regularity condition.

For a sequence $(v^n)_{n\geqslant 0}$, let $d_t^2 v^n$ denote the second difference quotient

$$d_t^2 v^n := \frac{1}{\tau}(d_t v^n - d_t v^{n-1}) = \frac{1}{\tau^2}(v^n - 2v^{n-1} + v^{n-2}), \quad n \geqslant 2.$$

The following lemma will be useful in the analysis; it presents a discrete version of the identity $\partial_t |v|^2 = 2\partial_t v \cdot v$.

Lemma 2.1 (discrete chain rule)**.** *For a sequence $(v^n)_{n\geqslant 0}$, we have*

$$2d_t v^n \cdot \widehat{v}^{n-1+\mu} = d_t|v^n|^2 - \mu\tau^2 d_t|d_t v^n|^2 - \mu\tau^3|d_t^2 v^n|^2 - (1-2\mu)\,\tau|d_t v^n|^2,$$

for $n \geqslant 2$.

Proof. We start by splitting the left-hand side of the asserted identity as

$$\begin{aligned} 2d_t v^n \cdot \widehat{v}^{n-1+\mu} &= 2d_t v^n \cdot v^{n-1/2} - 2d_t v^n \cdot (v^{n-1/2} - \widehat{v}^{n-1+\mu}) \\ &= d_t|v^n|^2 - 2\mu\tau d_t v^n \cdot (d_t v^n - d_t v^{n-1}) - (1-2\mu)\,\tau|d_t v^n|^2, \end{aligned}$$

where we have used the relation

$$\begin{aligned} v^{n-1/2} - \widehat{v}^{n-1+\mu} &= v^{n-1/2} - v^{n-1} - \mu\tau d_t v^{n-1} \\ &= \tau d_t v^n/2 - \mu\tau d_t v^{n-1} \\ &= \mu\tau(d_t v^n - d_t v^{n-1}) + (1/2-\mu)\,\tau d_t v^n. \end{aligned}$$

Note that

$$\begin{aligned} d_t v^n \cdot (d_t v^n - d_t v^{n-1}) &= \big(|d_t v^n|^2 - |d_t v^{n-1}|^2\big)/2 + \tau^2|d_t^2 v^n|^2/2 \\ &= \tau d_t|d_t v^n|^2/2 + \tau^2|d_t^2 v^n|^2/2; \end{aligned}$$

then, the desired result follows immediately. □

From Lemma 2.1 we deduce that, if $d_t u^n \cdot \widehat{u}^{n-1+\mu} = 0$, then

$$d_t|u^n|^2 = \mu\tau^2 d_t|d_t u^n|^2 + \mu\tau^3|d_t^2 u^n|^2 + (1-2\mu)\,\tau|d_t u^n|^2, \tag{15}$$

for all $n \geqslant 2$. Using this identity, in the following proposition, we establish the constraint violation property of the method.

Proposition 2.2 (constraint violation error)**.** *The sequence generated by Algorithm 2.1 satisfies, for all $m \geqslant 2$,*

$$|u^m|^2 - 1 = \mu\tau^2|d_t u^m|^2 + (1-\mu)\tau^2|d_t u^1|^2 + \mu\tau^4\sum_{n=2}^{m}|d_t^2 u^n|^2 + (1-2\mu)\tau^2\sum_{n=2}^{m}|d_t u^n|^2 \tag{16}$$

and

$$\begin{aligned} \||u^m|^2 - 1\|_{L^1} \leqslant \tau^2\Big(&\mu\|d_t u^m\|^2 + (1-\mu)\|d_t u^1\|^2 \\ &+ \mu\tau^2\sum_{n=2}^{m}\|d_t^2 u^n\|^2 + |1-2\mu|\sum_{n=2}^{m}\|d_t u^n\|^2\Big). \end{aligned} \tag{17}$$

Proof. Summing in (15) over n from $n=2$ to $n=m$ and multiplying the result by τ, we immediately obtain

$$|u^m|^2 - |u^1|^2 = \mu\tau^2\Big(|d_t u^m|^2 - |d_t u^1|^2 + \tau^2\sum_{n=2}^{m}|d_t^2 u^n|^2\Big) + (1-2\mu)\,\tau^2\sum_{n=2}^{m}|d_t u^n|^2.$$

As $|u^0|^2 = 1$ and u^1 is computed by the linearly implicit Euler method, we have $|u^1|^2 = |u^0|^2 + \tau^2|d_t u^1|^2 = 1 + \tau^2|d_t u^1|^2$, which yields (16). Integration of (16) over Ω then leads to the constraint violation relation (17). □

From Proposition 2.2, we immediately deduce the following properties:
(a) If $0 \leqslant \mu \leqslant 1/2$, then $|u^m| \geqslant 1$ almost everywhere in Ω.
(b) If $\mu = 0$, (16) reduces to the first-order constraint violation (10) of the linearly implicit Euler method.
(c) If $\mu = 1/2$ (midpoint and modified Euler methods), then (16) reduces to

$$|u^m|^2 - 1 = \frac{\tau^2}{2}\Big(|d_t u^m|^2 + |d_t u^1|^2 + \tau^2 \sum_{n=2}^{m} |d_t^2 u^n|^2\Big).$$

In the following proposition, we provide uniform upper bounds of the constraint violation error.

Proposition 2.3 (bound of the constraint violation error)**.** *Let $1/2 \leqslant \theta \leqslant 1$.*
(a) There exists $c_1 > 0$ such that $\||u^m|^2 - 1\|_{L^1} \leqslant c_1\tau$ for all $m \geqslant 2$ unconditionally.
(b) Let $\mu = 1/2$. There exists $c_2 > 0$ such that $\||u^m|^2 - 1\|_{L^1} \leqslant c_2\tau^2$ for $m \geqslant 2$ if and only if there exists $c > 0$ such that the discrete regularity property

$$\|d_t u^m\|^2 + \|d_t u^1\|^2 + \tau^2 \sum_{n=2}^{m} \|d_t^2 u^n\|^2 \leqslant c \tag{18}$$

is valid. The constants $c_1, c_2 > 0$ depend on the energy of u^0 and the constant $c_\star > 0$ in (13)*; c_2 depends also on the constant c in* (18)*.*

Proof. For all $n \geqslant 2$, the identity $\tau d_t^2 u^n = d_t u^n - d_t u^{n-1}$ implies

$$\tau^2\|d_t^2 u^n\|^2 \leqslant 2\big(\|d_t u^n\|^2 + \|d_t u^{n-1}\|^2\big),$$

and summation over n yields the inverse inequality

$$\tau^2 \sum_{n=2}^{m} \|d_t^2 u^n\|^2 \leqslant 4 \sum_{n=1}^{m} \|d_t u^n\|^2. \tag{19}$$

Combining the inverse inequality (19) with the energy stability (14) from Proposition 2.1, we see that the bound in (17) is of order τ unconditionally. If $\mu = 1/2$, by design, the bound is of order τ^2 if and only if the sharp discrete regularity condition (18) holds. □

The unconditional stability and the control of the constraint violation allow to apply weak compactness arguments and show the weak convergence of a subsequence of approximations toward a harmonic map; see, e.g., the proofs in [12, Ch. 7].

Remark 2.3 (beyond harmonic maps)**.** *The proposed approach is general and can be applied to a vast class of geometrically constrained partial differential equations. As an example, consider the LLG equation (see, e.g.,* [14, 6, 7, 21, 4]*)*

$$\partial_t m = -m \times \Delta m + \alpha\, m \times \partial_t m,$$

which models the dynamics of the magnetization m, a unit-length vector field, in ferromagnetic materials. Here, $\alpha > 0$ denotes the so-called Gilbert damping constant. Applying the approach to this problem leads to the following method: Given m^0 and m^1 (with m^1 computed by one step of the linearly implicit Euler method), for $n \geqslant 2$, set $\widehat{m}^{n-1+\mu} := m^{n-1} + \mu\tau \mathrm{d}_t m^{n-1}$ and compute $d_t m^n \in H^1_{\mathrm{D}}(\Omega;\mathbb{R}^\ell)$ such that $d_t m^n \cdot \widehat{m}^{n-1+\mu} = 0$ and

$$\alpha(d_t m^n, v) + (\widehat{m}^{n-1+\mu} \times d_t m^n, v) + (\nabla[m^{n-1} + \theta\tau d_t m^n], \nabla v) = 0$$

for all $v \in H^1_{\mathrm{D}}(\Omega;\mathbb{R}^\ell)$ *with* $v \cdot \widehat{m}^{n-1+\mu} = 0$. *Combining the analysis of this work with those in* [6, 1]*, one can show that the method is unconditionally stable, formally of second order in time if* $\theta = \mu = 1/2$*, and convergent toward a weak solution of the problem.*

2.3. **The linearly implicit two-step BDF method.** In this subsection, we recall the linearly implicit two-step BDF method for harmonic maps proposed in [2], along with its energy decay and constraint violation properties. This will provide the theoretical foundations for the experimental comparison of the algorithms carried out in Section 4.

The discrete time derivative $\dot{u}^n$ associated with the two-step backward difference formula (BDF2) is expressed as

$$\dot{u}^n = \frac{1}{2\tau}\big(3u^n - 4u^{n-1} + u^{n-2}\big).$$

Following [4], let $\widehat{u}^n := u^{n-1} + \tau d_t u^{n-1} = 2u^{n-1} - u^{n-2}$ be the extrapolated value at $t_n = n\tau$ of the linear interpolant based on (t_{n-2}, u^{n-2}) and (t_{n-1}, u^{n-1}). Notice that $\widehat{u}^n = \widehat{u}^{n-1+\mu}$ for $\mu = 1$ is an approximation to $u(t_n)$.

For the given initial value u^0, one can compute the second starting approximation u^1 by a single step method, for instance, by employing one step with the linearly implicit Euler method (6). Then, for given approximations u^{n-2} and u^{n-1}, we first seek $\dot{u}^n \in H^1_{\mathrm{D}}(\Omega;\mathbb{R}^\ell)$, satisfying the linearized unit-length condition $\dot{u}^n \cdot \widehat{u}^n = 0$, such that

$$(\dot{u}^n, v)_\star + \frac{1}{3}(\nabla[4u^{n-1} - u^{n-2} + 2\tau\dot{u}^n], \nabla v) = 0 \tag{20}$$

for all $v \in H^1_{\mathrm{D}}(\Omega;\mathbb{R}^\ell)$ with $v \cdot \widehat{u}^n = 0$. Notice that the new approximation

$$u^n := \frac{1}{3}(4u^{n-1} - u^{n-2} + 2\tau\dot{u}^n)$$

satisfies the required Dirichlet boundary condition $u^n|_{\Gamma_{\mathrm{D}}} = u_{\mathrm{D}}$, provided the approximations u^{n-2} and u^{n-1} satisfy this condition.

The algorithm of the BDF2 method [2] is summarized as follows.

Algorithm 2.2 (BDF2 method)**.** *Choose* $u^0 \in H^1(\Omega;\mathbb{R}^\ell)$ *with* $u^0|_{\Gamma_{\mathrm{D}}} = u_{\mathrm{D}}$ *and* $|u^0| = 1$.

(0) Compute $d_t u^1 \in H^1_{\mathrm{D}}(\Omega;\mathbb{R}^\ell)$ *such that* $d_t u^1 \cdot u^0 = 0$ *and*

$$(d_t u^1, v)_\star + (\nabla[u^0 + \tau d_t u^1], \nabla v) = 0$$

for all $v \in H^1_{\mathrm{D}}(\Omega;\mathbb{R}^\ell)$ *with* $v \cdot u^0 = 0$*; set* $u^1 = u^0 + \tau d_t u^1$ *and* $n = 2$.

(1) Set $\widehat{u}^n = 2u^{n-1} - u^{n-2}$ *and compute* $\dot{u}^n \in H^1_{\mathrm{D}}(\Omega;\mathbb{R}^\ell)$ *with* $\dot{u}^n \cdot \widehat{u}^n = 0$ *and*

$$(\dot{u}^n, v)_\star + \frac{1}{3}(\nabla[4u^{n-1} - u^{n-2} + 2\tau\dot{u}^n], \nabla v) = 0$$

for all $v \in H^1_{\mathrm{D}}(\Omega;\mathbb{R}^\ell)$ *with* $v \cdot \widehat{u}^n = 0$*; set* $u^n = (4u^{n-1} - u^{n-2} + 2\tau\dot{u}^n)/3$.

(2) Stop if $\|\dot{u}^n\|_\star + 2\tau\|\nabla\dot{u}^n\|/3 \leqslant \varepsilon_{stop}$ *or if* $n\tau \geqslant T$.

(3) Increase $n \to n+1$ *and continue with (1).*

Remark 2.4. *(i) Notice also that* (20) *can be written in the form*

$$(\dot{u}^n, v)_\star + (\nabla u^n, \nabla v) = 0$$

for all $v \in H^1_{\mathrm{D}}(\Omega;\mathbb{R}^\ell)$ *with* $v \cdot \widehat{u}^n = 0$.

(ii) Similarly to Algorithm 2.1, the first stopping criterion used in step (2) of Algorithm 2.2 is chosen in such a way that the following relationship holds

$$(\nabla u_h^{N_{stop}-1}, \nabla v) \approx R(v) \text{ for all admissible } v \quad \text{and} \quad \|R\|_{H^1(\Omega)^\star} \leqslant \varepsilon_{stop}. \tag{21}$$

Note that the first condition in (12) *holds with equality sign for the implicit Euler, modified Euler, and midpoint methods, while the first condition in* (21) *holds approximately for the BDF2 method. The aim is to ensure a fair comparison of all four methods in numerical experiments.*

We now recall the main properties of the BDF2 method established in [2]:
(i) *Energy decay property*: Let $G \in \mathbb{R}^{2\times 2}$ be the positive definite, symmetric matrix given by

$$G := \frac{1}{4}\begin{pmatrix} 5 & -2 \\ -2 & 1 \end{pmatrix}.$$

Let $\mathcal{U}^n = (u^n, u^{n-1})^\top$ and let $\|\cdot\|_G$ be a BDF-adapted variant of the L^2 norm,

$$\|\mathcal{U}^n\|_G^2 = (G\mathcal{U}^n, \mathcal{U}^n) = \frac{5}{4}\|u^n\|^2 - (u^n, u^{n-1}) + \frac{1}{4}\|u^{n-1}\|^2.$$

Then, the BDF2 method satisfies the following energy identity (G-stability) for all $m \geqslant 2$

$$\|\nabla\mathcal{U}^m\|_G^2 + \tau\sum_{n=2}^{m}\|\dot{u}^n\|_\star^2 + \frac{\tau^4}{4}\sum_{n=2}^{m}\|d_t^2\nabla u^n\|^2 = \|\nabla\mathcal{U}^1\|_G^2.$$

Constraint violation result: If u^1 is computed by the linearly implicit Euler method (6), the sequence $(|u^n|)_{n\geqslant 1}$ is increasing almost everywhere in Ω, and we have the following constraint violation result: For all $m \geqslant 2$, it holds that

$$\big\||u^m|^2 - 1\big\|_{L^1} = \frac{3}{2}\Big(1 - \frac{1}{3^m}\Big)\tau^2\|d_t u^1\|^2 + \frac{3}{2}\tau^4\sum_{n=2}^{m}\Big(1 - \frac{1}{3^{m+1-n}}\Big)\|d_t^2 u^n\|^2. \tag{22}$$

It follows that $\big\||u^m|^2 - 1\big\|_{L^1} \leqslant c_p\tau^p$ unconditionally for $p = 1$. The result holds for $p = 2$ under the sharp discrete regularity condition

$$\|d_t u^1\|^2 + \tau^2\sum_{n=2}^{m}\|d_t^2 u^n\|^2 \leqslant c. \tag{23}$$

3. Variable step sizes

In this section, we extend the (θ, μ)-method to allow for variable step sizes, aiming to improve the accuracy of the numerical solutions near singularities (e.g., a singularity at $t = 0$ for nonsmooth initial data or a finite time blow-up even for smooth initial data) and to apply acceleration techniques to speed up the convergence to stationary states, retaining the unconditional energy stability and the constraint violation properties. The analysis of the BDF2 method depends crucially on its G-stability property; cf. [2]; consequently, the extension to variable step sizes is cumbersome.

In this section, we set $t_0 := 0$, and, for given positive step sizes $(\tau_n)_{n\geqslant 1}$, we define the nodes $t_n := t_{n-1} + \tau_n$, $n \geqslant 1$. Using this notation, we denote by

$$d_t u^n := \frac{u^n - u^{n-1}}{\tau_n}$$

the backward difference quotient.

For given starting approximation u^0, we compute u^1 by one step of the implicit Euler method: First, we determine $d_t u^1 \in H^1_{\mathrm{D}}(\Omega;\mathbb{R}^\ell)$, satisfying the linearized unit-length condition $d_t u^1 \cdot u^0 = 0$, such that

$$(d_t u^1, v)_\star + (\nabla u^0 + \tau_1\nabla d_t u^1, \nabla v) = 0 \tag{24}$$

for all $v \in H^1_{\mathrm{D}}(\Omega;\mathbb{R}^\ell)$ with $v \cdot u^0 = 0$. Then, we define $u^1 := u^0 + \tau_1 d_t u^1$.

Next, for $n \geqslant 2$, let $s_n := \tau_n/\tau_{n-1}$ denote the ratio of two consecutive step sizes. For given approximations u^{n-2} and u^{n-1}, and $0 \leqslant \mu \leqslant 1$, let

$$\widehat{u}^{n-1+\mu} := (1+\mu s_n)u^{n-1} - \mu s_n u^{n-2} = u^{n-1} + \mu\tau_n d_t u^{n-1}$$

be the extrapolated value at $t_{n-1+\mu} = t_{n-1} + \mu\tau_n$ of the linear interpolant based on (t_{n-2}, u^{n-2}) and (t_{n-1}, u^{n-1}). Then, seek $d_t u^n \in H^1_{\mathrm{D}}(\Omega;\mathbb{R}^\ell)$, satisfying the linearized unit-length condition $d_t u^n \cdot \widehat{u}^{n-1+\mu} = 0$, such that

$$(d_t u^n, v)_\star + (\nabla\big[u^{n-1} + \theta\tau_n d_t u^n\big], \nabla v) = 0 \tag{25}$$

for all $v \in H^1_{\mathrm{D}}(\Omega;\mathbb{R}^\ell)$ with $v \cdot \widehat{u}^{n-1+\mu} = 0$. Here, $0 < \theta \leqslant 1$. Thus, having computed $d_t u^n$, we define the new approximation $u^n := u^{n-1} + \tau_n d_t u^n$ that satisfies the required Dirichlet boundary condition $u^n|_{\Gamma_{\mathrm{D}}} = u_{\mathrm{D}}$, provided the approximation u^{n-1} at the previous step satisfies this condition.

Remark 3.1. *Similarly as the (θ,μ)-method* (11) *with constant step size for harmonic maps,* (25) *reduces to*

(i) the linearly implicit Euler method for $\theta = 1$ and $\mu = 0$;
(ii) the linearly implicit midpoint method for $\theta = 1/2$ and $\mu = 1/2$;
(iii) a modified linearly implicit Euler method for $\theta = 1$ and $\mu = 1/2$.

We now extend the analysis of the previous section to the case of variable step sizes. We discuss the energy decay and constraint violation properties of the method. It can be proved that the iteration (25) becomes stationary for $n \to \infty$.

We begin with the discrete energy law satisfied by the approximations.

Proposition 3.1 (energy decay)**.** *For the (θ,μ)-method* (25) *and $m \geqslant 2$, if u^1 is computed by the linearly implicit Euler method* (24)*, we have*

$$\frac{1}{2}\|\nabla u^m\|^2 + \sum_{n=1}^{m}\tau_n\|d_t u^n\|_\star^2 + \frac{\tau_1^2}{2}\|\nabla d_t u^1\|^2 + \left(\theta - \frac{1}{2}\right)\sum_{n=2}^{m}\tau_n^2\|\nabla d_t u^n\|^2 = \frac{1}{2}\|\nabla u^0\|^2. \tag{26}$$

The proof is analogous to the one of Proposition 2.1 and is therefore omitted.

We now study the constraint violation properties. In the case of variable step sizes, the second difference quotient $d_t^2 u^n$ is defined by

$$d_t^2 u^n := \frac{1}{\tau_n}(d_t u^n - d_t u^{n-1}), \quad n \geqslant 2. \tag{27}$$

We have the following analogue of Lemma 2.1.

Lemma 3.1 (discrete chain rule)**.** *For a sequence $(v^n)_{n\geqslant 0}$ and $n \geqslant 2$ we have*

$$2d_t v^n \cdot \widehat{v}^{n-1+\mu} = d_t|v^n|^2 - \mu\tau_n^2 d_t|d_t v^n|^2 - \mu\tau_n^3|d_t^2 v^n|^2 - (1-2\mu)\,\tau_n|d_t v^n|^2.$$

We omit the proof as it follows along the lines of that of Lemma 2.1. Lemma 3.1 implies that, if $d_t u^n \cdot \widehat{u}^{n-1+\mu} = 0$, for $n \geqslant 2$ we have

$$d_t|u^n|^2 = \mu\tau_n^2 d_t|d_t u^n|^2 + \mu\tau_n^3|d_t^2 u^n|^2 + (1-2\mu)\tau_n|d_t u^n|^2. \tag{28}$$

This relation is the crucial ingredient for the identity established in the following proposition.

Proposition 3.2 (constraint violation error)**.** *For the (θ,μ)-method* (25) *and $m \geqslant 2$, if $|u^0| = 1$ and u^1 is computed by the linearly implicit Euler method* (24)*, we have*

$$
\begin{aligned}
|u^m|^2 - 1 = \mu\tau_m^2|d_t u^m|^2 + (1-\mu)\tau_1^2|d_t u^1|^2 + \mu\sum_{n=1}^{m-1}\tau_n^2(1-s_{n+1}^2)|d_t u^n|^2 \\
+ \mu\sum_{n=2}^{m}\tau_n^4|d_t^2 u^n|^2 + (1-2\mu)\sum_{n=2}^{m}\tau_n^2|d_t u^n|^2.
\end{aligned} \tag{29}
$$

Thus, we have the constraint violation estimate

$$
\begin{aligned}
\||u^m|^2 - 1\|_{L^1} \leqslant \mu\tau_m^2\|d_t u^m\|^2 + (1-\mu)\tau_1^2\|d_t u^1\|^2 + \mu\sum_{n=1}^{m-1}\tau_n^2|1-s_{n+1}^2|\|d_t u^n\|^2 \\
+ \mu\sum_{n=2}^{m}\tau_n^4\|d_t^2 u^n\|^2 + |1-2\mu|\sum_{n=2}^{m}\tau_n^2\|d_t u^n\|^2.
\end{aligned} \tag{30}
$$

Proof. We multiply (28) by τ_n and write it in the form

$$
|u^n|^2 - |u^{n-1}|^2 = \mu\tau_n^2\big(|d_t u^n|^2 - |d_t u^{n-1}|^2\big) + \mu\tau_n^4|d_t^2 u^n|^2 + (1-2\mu)\,\tau_n^2|d_t u^n|^2.
$$

Summing over n from $n=2$ to $n=m$, we obtain

$$
\begin{aligned}
|u^m|^2 - |u^1|^2 = \mu\sum_{n=2}^{m}\tau_n^2\big(|d_t u^n|^2 - |d_t u^{n-1}|^2\big) \\
+ \mu\sum_{n=2}^{m}\tau_n^4|d_t^2 u^n|^2 + (1-2\mu)\sum_{n=2}^{m}\tau_n^2|d_t u^n|^2.
\end{aligned}
$$

Shifting the indices in the sum and using the definition of the step size ratio ($s_{n+1} = \tau_{n+1}/\tau_n$), the first term on the right-hand side can be rewritten as

$$
\sum_{n=2}^{m}\tau_n^2\big(|d_t u^n|^2 - |d_t u^{n-1}|^2\big) = \tau_m^2|d_t u^m|^2 - \tau_2^2|d_t u^1|^2 + \sum_{n=2}^{m-1}\tau_n^2(1-s_{n+1}^2)|d_t u^n|^2.
$$

We thus obtain

$$
\begin{aligned}
&|u^m|^2 - |u^1|^2 \\
&\quad = \mu\Big(\tau_m^2|d_t u^m|^2 - \tau_2^2|d_t u^1|^2 + \sum_{n=2}^{m-1}\tau_n^2(1-s_{n+1}^2)|d_t u^n|^2 + \sum_{n=2}^{m}\tau_n^4|d_t^2 u^n|^2\Big) \\
&\qquad + (1-2\mu)\sum_{n=2}^{m}\tau_n^2|d_t u^n|^2.
\end{aligned}
$$

If $|u^0| = 1$ and u^1 is computed by the implicit Euler method, then $|u^1|^2 = |u^0|^2 + \tau_1^2|d_t u^1|^2 = 1 + \tau_1^2|d_t u^1|^2$, which yields (29). Taking the L^1 norm, we obtain the constraint violation estimate (30). □

Remark 3.2. *(i) Notice that in the case of constant step size, we have $s_n = 1$ for all $n \geqslant 2$, and the bound in the constraint violation estimate* (30) *reduces to the expression on the right-hand side of* (17)*.*
(ii) If $0 \leqslant \mu \leqslant 1/2$ and if the step size monotonically decreases, i.e., if $s_n \leqslant 1$ for all

$2 \leqslant n \leqslant m$, *it follows from* (29) *that* $|u^m| \geqslant 1$.
(iii) From (29), *for* $\mu = 0$, *we obtain the constraint violation identity*

$$|u^m|^2 - 1 = \sum_{n=1}^{m} \tau_n^2 |d_t u^n|^2$$

of the implicit Euler method. For $\mu = 1/2$, *we obtain the constraint violation identity*

$$|u^m|^2 - 1 = \frac{1}{2}\left(\tau_1^2 |d_t u^1|^2 + \tau_m^2 |d_t u^m|^2 + \sum_{n=1}^{m-1} \tau_n^2 (1 - s_{n+1}^2) |d_t u^n|^2 + \sum_{n=2}^{m} \tau_n^4 |d_t^2 u^n|^2 \right)$$

of the midpoint and modified Euler methods.

4. Numerical experiments

We illustrate the accuracy in approximating the unit-length constraint and the overall performance of the proposed (θ, μ)-method (Algorithm 2.1) through a series of numerical experiments in two dimensions, comparing it with the BDF2 method (Algorithm 2.2). Moreover, for the (θ, μ)-method, we present numerical results obtained using variable step sizes.

In all computations, the domain of the problem is $\Omega = (-1/2, 1/2)^2$ with $\Gamma_{\mathrm{D}} = \partial\Omega$, and the vector fields attain values in $\mathbb{R}^3$. For the spatial discretization, we consider a fixed unstructured triangular mesh $\mathcal{T}_h$ of Ω generated by Netgen [30] (consisting of 4901 vertices and 9544 triangles, and having mesh size $h \approx 2.287 \cdot 10^{-2}$). For the approximation of vector-valued functions, we use H^1-conforming first-order finite elements, i.e., we consider the space $V_h \subset H^1(\Omega; \mathbb{R}^3)$ of vector-valued $\mathcal{T}_h$-piecewise affine and globally continuous functions. The pointwise orthogonality imposed in the variational formulation of the methods is enforced only at the vertices of $\mathcal{T}_h$. For all methods, the solution of the arising constrained linear system is based on the null-space method given in [29, 27]. Moreover, we consider a fixed tolerance $\varepsilon_{\mathrm{stop}} = 10^{-6}$ or a fixed final time $T = 1$ in the stopping criterion of step (2).

4.1. Constant step size.

We start with a collection of numerical experiments to assess the performance of the schemes in the case of constant step size.

4.1.1. *Comparison of Algorithms 2.1 and 2.2 (H^1-gradient flow).* We consider the model problem from [2, Section 4.1]. Let $u_{\mathrm{D}} = \pi_{\mathrm{st}}^{-1}|_{\Gamma_{\mathrm{D}}}$, where

$$\pi_{\mathrm{st}}^{-1}(x) = (|x|^2 + 1)^{-1}(2x, 1 - |x|^2)^{\top} \tag{31}$$

denotes the inverse stereographic projection. It is well known that $u = \pi_{\mathrm{st}}^{-1}$ is a harmonic map with $u|_{\Gamma_{\mathrm{D}}} = u_{\mathrm{D}}$.

The discrete Dirichlet data are obtained interpolating the exact solution on the boundary. To initialize the iterative algorithms, we consider a fixed initial guess $u_h^0 = \mathcal{I}_h u^0$, where $\mathcal{I}_h : C(\overline{\Omega}; \mathbb{R}^3) \to V_h$ denotes the nodal interpolation operator (or its scalar-valued counterpart) and

$$u^0(x) = \big([u_1(x) + \varphi(x)]^2 + [u_2(x) - \varphi(x)]^2 + u_3(x)^2\big)^{-1/2} \begin{pmatrix} u_1(x) + \varphi(x) \\ u_2(x) - \varphi(x) \\ u_3(x) \end{pmatrix} \tag{32}$$

with

$$\varphi(x) = 16 \sin(4\pi x_1)(x_1^2 - 1/4)(x_2^2 - 1/4).$$

In our first numerical experiment, we compare the proposed (θ, μ)-method and the BDF2 method for the case of the H^1-gradient flow, i.e., $(\cdot, \cdot)_\star = (\nabla \cdot, \nabla \cdot)$, considering the

step sizes $\tau = 2^{-m}$ for $m = 4, \dots, 10$. For the (θ, μ)-method, we consider the relevant cases of the implicit Euler method ($\theta = 1$, $\mu = 0$) and the midpoint method ($\theta = 1/2$, $\mu = 1/2$). The results are displayed in Table 1. We compare the algorithms and test their convergence with respect to τ by assessing the following quantities:

- N_{stop}, the number of iterations required to meet the tolerance;
- $\delta_\infty[u_h^{N_{\mathrm{stop}}}] := \| |u_h^{N_{\mathrm{stop}}}| - 1 \|_{L^\infty}$, the constraint violation error, measured using the L^∞-norm (not unconditionally controlled by the algorithms);
- $\delta_{\mathrm{uni}}[u_h^{N_{\mathrm{stop}}}] := \| \mathcal{I}_h |u_h^{N_{\mathrm{stop}}}|^2 - 1 \|_{L^1}$, the constraint violation error, measured using the L^1-norm (this is the quantity that should decay linearly for the implicit Euler method and, under a sharp discrete regularity condition, quadratically for the BDF2 method and the midpoint method);
- A^2, B^2, and C^2, the quantities that, if uniformly bounded with respect to τ, guarantee the second-order convergence of $\delta_{\mathrm{uni}}[u_h^{N_{\mathrm{stop}}}]$ as $\tau \to 0$ for the BDF2 method (see (23)) and the midpoint method (see (18)). Specifically, we have

$$A^2 = \tau^2 \sum_{n=2}^{N_{\mathrm{stop}}} \|d_t^2 u_h^n\|^2, \quad B^2 = \|d_t u_h^1\|^2, \quad \text{and} \quad C^2 = \|d_t u_h^{N_{\mathrm{stop}}}\|^2.$$

  Note that C^2 is relevant only for the midpoint method, and that none of these quantities plays a role in the analysis of the implicit Euler method;
- $\delta_{\mathrm{ener}}[u_h^{N_{\mathrm{stop}}}] = |I[u_h^{N_{\mathrm{stop}}}] - I[u]|$, the energy approximation error.

Finally, eoc_∞ and $\mathrm{eoc}_{\mathrm{uni}}$ denote the experimental rates q of the convergences of $\delta_\infty[u_h^{N_{\mathrm{stop}}}]$ and $\delta_{\mathrm{uni}}[u_h^{N_{\mathrm{stop}}}]$ as $\tau \to 0$, respectively, computed as logarithmic slopes

$$q = -\log(\mathrm{err}_{k+1}/\mathrm{err}_k)/\log 2$$

for any two consecutive instances of the errors.

Looking at Table 1, we see that $N_{\mathrm{stop}} \propto \tau^{-1}$ for all algorithms. For any fixed τ, the algorithms require approximately the same number of iterations to satisfy the stopping criterion. In particular, for the BDF2 and the midpoint methods, the number of iterations is almost identical. For the implicit Euler method, we see a clear first-order convergence of the L^1-error (as expected from the theory). We also see a first-order convergence of the L^∞-error. For the BDF2 method and the midpoint method, we observe a second-order convergence of the constraint violation error measured in both the L^1-norm and the L^∞-norm. The midpoint method is slightly more accurate, in the sense that for each value of τ the constraint violation error is about $1/3$ of the one of the BDF2 method. The quantities A^2, B^2 (and C^2 for the midpoint method) stay uniformly bounded as $\tau \to 0$, which is a numerical validation of the discrete regularity property. For both methods, the quantity A^2 converges linearly to 0 as $\tau \to 0$. The energy approximation error decays for the implicit Euler method, whereas it stabilizes at about $2.8 \cdot 10^{-4}$ for both the BDF method and the midpoint method. We believe that the lack of convergence of the energy error as $\tau \to 0$ for the higher-order methods is due to the spatial approximation error becoming predominant.

In Fig. 1, for both the BDF2 method and the midpoint method, we show the evolution of the energy and the constraint violation L^1-error during the iteration for $\tau = 2^{-5}$. On the one hand, we see that the energetic behavior of the methods is very similar, as the curves are nearly superimposed (for $\tau = 2^{-5}$ the difference between the energy values obtained with the two schemes is of the order of 0.01%). For both methods, the energy monotonically decays in an exponential fashion and converges to the approximate energy value of the inverse stereographic projection. On the other hand, the behavior of the

Implicit Euler method							
τ	N_{stop}	$\delta_\infty[u_h^{N_{\text{stop}}}]$	eoc_∞	$\delta_{\text{uni}}[u_h^{N_{\text{stop}}}]$	eoc_{uni}	$\delta_{\text{ener}}[u_h^{N_{\text{stop}}}]$	
2^{-4}	274	1.068e−2	—	4.790e−3	—	1.757e−2	
2^{-5}	535	5.445e−3	0.9716	2.436e−3	0.9755	8.420e−3	
2^{-6}	1057	2.750e−3	0.9856	1.228e−3	0.9876	4.008e−3	
2^{-7}	2101	1.382e−3	0.9928	6.169e−4	0.9938	1.846e−3	
2^{-8}	4190	6.926e−4	0.9964	3.091e−4	0.9969	7.775e−4	
2^{-9}	8368	3.468e−4	0.9982	1.547e−4	0.9984	2.460e−4	
2^{-10}	16723	1.735e−4	0.9991	7.741e−5	0.9992	1.904e−5	

BDF2 method								
τ	N_{stop}	$\delta_\infty[u_h^{N_{\text{stop}}}]$	eoc_∞	$\delta_{\text{uni}}[u_h^{N_{\text{stop}}}]$	eoc_{uni}	$\delta_{\text{ener}}[u_h^{N_{\text{stop}}}]$	A^2	B^2
2^{-4}	262	1.449e−3	—	6.915e−4	—	2.106e−3	3.771e−3	1.134e−1
2^{-5}	523	3.778e−4	1.940	1.805e−4	1.937	3.342e−4	1.988e−3	1.204e−1
2^{-6}	1046	9.649e−5	1.969	4.615e−5	1.968	1.260e−4	1.019e−3	1.242e−1
2^{-7}	2090	2.439e−5	1.984	1.167e−5	1.984	2.437e−4	5.153e−4	1.261e−1
2^{-8}	4179	6.131e−6	1.992	2.934e−6	1.992	2.735e−4	2.591e−4	1.271e−1
2^{-9}	8357	1.537e−6	1.996	7.356e−7	1.996	2.810e−4	1.299e−4	1.276e−1
2^{-10}	16712	3.848e−7	1.998	1.842e−7	1.998	2.829e−4	6.505e−5	1.278e−1

midpoint method									
τ	N_{stop}	$\delta_\infty[u_h^{N_{\text{stop}}}]$	eoc_∞	$\delta_{\text{uni}}[u_h^{N_{\text{stop}}}]$	eoc_{uni}	$\delta_{\text{ener}}[u_h^{N_{\text{stop}}}]$	A^2	B^2	C^2
2^{-4}	263	4.841e−4	—	2.308e−4	—	5.069e−4	3.908e−3	1.134e−1	7.338e−15
2^{-5}	524	1.260e−4	1.942	6.019e−5	1.939	7.805e−5	2.022e−3	1.204e−1	7.967e−15
2^{-6}	1046	3.217e−5	1.970	1.538e−5	1.968	2.311e−4	1.027e−3	1.242e−1	8.307e−15
2^{-7}	2090	8.129e−6	1.984	3.890e−6	1.984	2.703e−4	5.174e−4	1.261e−1	8.484e−15
2^{-8}	4179	2.044e−6	1.992	9.780e−7	1.992	2.802e−4	2.596e−4	1.271e−1	8.514e−15
2^{-9}	8357	5.123e−7	1.996	2.452e−7	1.996	2.827e−4	1.300e−4	1.276e−1	8.529e−15
2^{-10}	16712	1.283e−7	1.998	6.139e−8	1.998	2.833e−4	6.508e−5	1.278e−1	8.552e−15

TABLE 1. Comparison of the implicit Euler, BDF2 and midpoint methods (H^1-gradient flow).

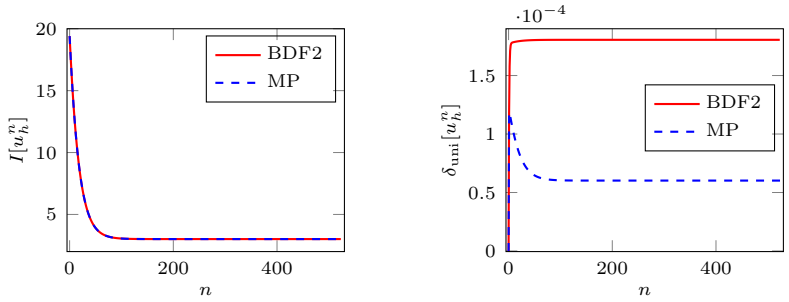

FIGURE 1. Evolution of the energy (left) and the constraint violation L^1-error (right) for the approximations generated by the BDF2 and the midpoint (MP) methods (H^1-gradient flow, $\tau = 2^{-5}$).

schemes is clearly different as far as the evolution of the constraint violation error is concerned. While the error is monotonically increasing for the BDF2 method (as expected from the theory, see (22)), for the midpoint method it reaches its maximal value in the very first iteration, and then decays monotonically until it stabilizes to its final value. For the sake of readability, in the plots we have omitted the results for the implicit Euler method. However, we report that the energetic behavior is very similar, whereas the constraint violation error, in agreement with (10), has the same monotonically increasing behavior of the BDF2 method (but the value is one order of magnitude larger).

4.1.2. *Comparison of Algorithms 2.1 and 2.2 (L^2-gradient flow).* We repeat the experiment of Section 4.1.1 for the implicit Euler, midpoint, and BDF2 methods, this time focusing on the L^2-gradient flow (i.e., $(\cdot,\cdot)_\star = (\cdot,\cdot)$) instead of the H^1-gradient flow. The

spatial discretization and the stopping tolerance are the same as before, while we consider the values $\tau = 2^{-m}$ for $m = 10, \dots, 16$ for the step size.

Implicit Euler method						
τ	N_{stop}	$\delta_\infty[u_h^{N_{\text{stop}}}]$	eoc_∞	$\delta_{\text{uni}}[u_h^{N_{\text{stop}}}]$	eoc_{uni}	$\delta_{\text{ener}}[u_h^{N_{\text{stop}}}]$
2^{-10}	358	2.718e−2	—	1.419e−2	—	6.182e−2
2^{-11}	704	1.430e−2	0.9268	7.535e−3	0.9132	2.920e−2
2^{-12}	1394	7.338e−3	0.9622	3.895e−3	0.9520	1.396e−2
2^{-13}	2776	3.719e−3	0.9807	1.982e−3	0.9743	6.697e−3
2^{-14}	5538	1.872e−3	0.9902	1.001e−3	0.9865	3.170e−3
2^{-15}	11063	9.392e−4	0.9951	5.027e−4	0.9931	1.434e−3
2^{-16}	22113	4.704e−4	0.9975	2.519e−4	0.9965	5.726e−4

BDF2 method								
τ	N_{stop}	$\delta_\infty[u_h^{N_{\text{stop}}}]$	eoc_∞	$\delta_{\text{uni}}[u_h^{N_{\text{stop}}}]$	eoc_{uni}	$\delta_{\text{ener}}[u_h^{N_{\text{stop}}}]$	A^2	B^2
2^{-10}	347	1.609e−2	—	7.327e−3	—	3.100e−2	6.151e2	4.441e3
2^{-11}	691	5.912e−3	1.444	2.319e−3	1.660	8.393e−3	5.269e2	5.857e3
2^{-12}	1382	2.111e−3	1.486	6.787e−4	1.772	2.097e−3	3.977e2	7.058e3
2^{-13}	2763	7.093e−4	1.574	1.876e−4	1.855	3.567e−4	2.692e2	7.954e3
2^{-14}	5526	2.237e−4	1.664	4.983e−5	1.913	1.151e−4	1.670e2	8.552e3
2^{-15}	11051	6.862e−5	1.705	1.290e−5	1.949	2.400e−4	9.726e1	8.918e3
2^{-16}	22101	2.068e−5	1.731	3.291e−6	1.971	2.724e−4	5.438e1	9.128e3

midpoint method									
τ	N_{stop}	$\delta_\infty[u_h^{N_{\text{stop}}}]$	eoc_∞	$\delta_{\text{uni}}[u_h^{N_{\text{stop}}}]$	eoc_{uni}	$\delta_{\text{ener}}[u_h^{N_{\text{stop}}}]$	A^2	B^2	C^2
2^{-10}	347	5.514e−3	—	2.491e−3	—	8.888e−3	7.141e2	4.441e3	9.241e−13
2^{-11}	692	2.013e−3	1.454	7.798e−4	1.675	2.439e−3	5.826e2	5.857e3	9.678e−13
2^{-12}	1382	7.107e−4	1.502	2.271e−4	1.780	4.910e−4	4.258e2	7.058e3	9.953e−13
2^{-13}	2764	2.372e−4	1.583	6.263e−5	1.858	7.187e−5	2.818e2	7.954e3	9.896e−13
2^{-14}	5526	7.469e−5	1.667	1.662e−5	1.914	2.275e−4	1.721e2	8.552e3	9.974e−13
2^{-15}	11051	2.291e−5	1.705	4.302e−6	1.950	2.690e−4	9.924e1	8.918e3	9.987e−13
2^{-16}	22101	6.905e−6	1.730	1.097e−6	1.971	2.798e−4	5.516e1	9.128e3	9.994e−13

TABLE 2. Comparison of the implicit Euler, BDF2 and midpoint methods (L^2-gradient flow).

The results of the simulations are displayed in Table 2. For the implicit Euler method, the expected linear decay of the constraint violation error (measured both with respect to the L^1-norm and the L^∞-norm) is clearly visible. However, differently from what we observed for the H^1-gradient flow, this behavior emerges only for the smallest step sizes (there is a much longer preasymptotic phase than for the H^1-gradient flow). The energy approximation error converges to 0 linearly as $\tau \to 0$. In terms of accuracy, the performance of the H^1-gradient flow is significantly better, e.g., the smallest constraint violation error obtained with the L^2-gradient flow, $\delta_{\text{uni}}[u_h^{N_{\text{stop}}}] = 2.519 \cdot 10^{-4}$, requires $\tau = 2^{-16}$ and 22113 iterations. With the H^1-gradient flow, the choice $\tau = 2^{-9}$ results only in 8368 iterations and leads to a smaller error ($\delta_{\text{uni}}[u_h^{N_{\text{stop}}}] = 1.547 \cdot 10^{-4}$).

A long preasymptotic phase is observed also for the BDF2 method with L^2-gradient flow (much longer than for the version with H^1-gradient flow). Indeed, the quadratic convergence guaranteed by the method is (almost) seen only for the smallest step sizes. On the other hand, as we saw for the case of the H^1-gradient flow, the convergence of the energy approximation is spoiled by the spatial approximation error. A difference between the two considered gradient flow metrics is visible also looking at the order of magnitude of A^2 and B^2, with the values for the L^2-gradient flow being significantly larger than those for the H^1-gradient flow. The quantity A^2 tends to 0 as τ increases, whereas we can observe a slight growth of B^2.

Similarly, in the case of the midpoint method, we see the expected second-order convergence of the L^1-error only when the step size becomes sufficiently small. Again, the energy approximation error does not converge. The quantity A^2 tends to 0 as τ decreases, whereas we can observe a slight growth of both B^2 and C^2.

4.1.3. *Modified implicit Euler method.* We repeat the experiment for the modified implicit Euler method (Algorithm 2.1 with $\theta = 1$ and $\mu = 1/2$), considering both the H^1-gradient flow and the L^2-gradient flow. The modified implicit Euler method is a mixture of the standard Euler and midpoint methods, for which the variational formulation to be solved at each iteration is the one of the standard Euler method. However, like in the midpoint method, for $n \geqslant 2$, the orthogonality constraint is considered with respect to extrapolated value $\widehat{u}_h^{n-1/2}$, instead of u_h^{n-1}.

Modified implicit Euler method (H^1-gradient flow)									
τ	N_{stop}	$\delta_\infty[u_h^{N_{\text{stop}}}]$	eoc_∞	$\delta_{\text{uni}}[u_h^{N_{\text{stop}}}]$	eoc_{uni}	$\delta_{\text{ener}}[u_h^{N_{\text{stop}}}]$	A^2	B^2	C^2
2^{-4}	271	4.830e−4	—	2.304e−4	—	5.055e−4	3.706e−3	1.134e−1	7.037e−15
2^{-5}	532	1.259e−4	1.940	6.016e−5	1.937	7.815e−5	1.966e−3	1.204e−1	7.795e−15
2^{-6}	1054	3.216e−5	1.969	1.538e−5	1.968	2.311e−4	1.012e−3	1.242e−1	8.216e−15
2^{-7}	2099	8.129e−6	1.984	3.890e−6	1.984	2.703e−4	5.136e−4	1.261e−1	8.318e−15
2^{-8}	4187	2.044e−6	1.992	9.780e−7	1.992	2.802e−4	2.587e−4	1.271e−1	8.490e−15
2^{-9}	8365	5.123e−7	1.996	2.452e−7	1.996	2.827e−4	1.298e−4	1.276e−1	8.517e−15
2^{-10}	16721	1.283e−7	1.998	6.139e−8	1.998	2.833e−4	6.502e−5	1.278e−1	8.530e−15

Modified implicit Euler method (L^2-gradient flow)									
τ	N_{stop}	$\delta_\infty[u_h^{N_{\text{stop}}}]$	eoc_∞	$\delta_{\text{uni}}[u_h^{N_{\text{stop}}}]$	eoc_{uni}	$\delta_{\text{ener}}[u_h^{N_{\text{stop}}}]$	A^2	B^2	C^2
2^{-10}	347	5.462e−3	—	2.461e−3	—	8.764e−3	6.533e2	4.441e3	9.186e−13
2^{-11}	700	1.996e−3	1.453	7.757e−4	1.666	2.423e−3	5.499e2	5.857e3	9.657e−13
2^{-12}	1390	7.109e−4	1.489	2.266e−4	1.775	4.892e−4	4.106e2	7.058e3	9.945e−13
2^{-13}	2772	2.380e−4	1.579	6.258e−5	1.857	7.205e−5	2.756e2	7.954e3	9.894e−13
2^{-14}	5534	7.495e−5	1.667	1.662e−5	1.913	2.275e−4	1.699e2	8.552e3	9.973e−13
2^{-15}	11059	2.296e−5	1.707	4.302e−6	1.950	2.690e−4	9.854e1	8.918e3	9.987e−13
2^{-16}	22109	6.912e−6	1.732	1.097e−6	1.971	2.798e−4	5.496e1	9.128e3	9.994e−13

TABLE 3. Performance of the modified implicit Euler method (H^1- and L^2-gradient flows).

The results of the simulations are displayed in Table 3. Comparing the performance of this method for both gradient flow metrics with the previous three approaches, we can see that the modified implicit Euler method behaves like the midpoint method.

4.1.4. *Performance in the presence of singularities.* It is well known that the heat flow of harmonic maps can develop singularities, even if the initial value is smooth. In this subsection, we test the performance of the projection-free linearly implicit midpoint method in such a situation.

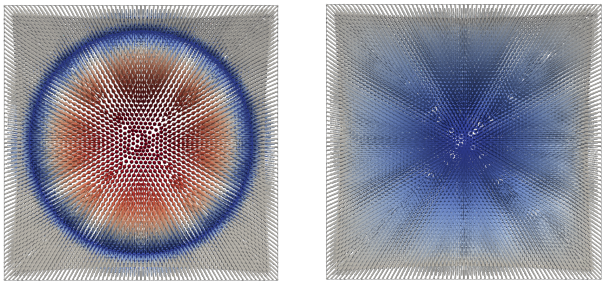

(A) Initial value. (B) Final value.

FIGURE 2. Pictures of the initial value (left) and the final value (right). The picture of the final value refers to the results obtained for $\tau = 2^{-14}$. The color scale refers to the third component of the field, which attains values between -1 (blue) and 1 (red).

The problem specifications are the same as in the previous experiments, except for the initial value and the stopping criterion. We consider the initial value [19]

$$u^0(x) = |x|^{-1}\big(x \sin \phi(2|x|), |x| \cos \phi(2|x|)\big)^\top \tag{33}$$

with $\phi(s) = (3\pi/2)\min\{s^2, 1\}$. We refer to [13, Section 6.2] for numerical results for the harmonic map heat flow with this initial value obtained with the linearly implicit Euler method (6). Restricting ourselves to the L^2-gradient flow and the midpoint method, we simulate the gradient flow dynamics in the fixed time interval $[0, T]$ with $T = 1$ using the values $\tau = 2^{-m}$ for $m = 11, \dots, 16$ for the step size. For pictures of the initial value u_h^0 and the final value u_h^N (with $N = 2^m$) computed by the algorithm for the case $m = 14$, we refer to Fig. 2.

midpoint method								
τ	N	$\delta_\infty[u_h^N]$	eoc_∞	$\delta_{\mathrm{uni}}[u_h^N]$	$\mathrm{eoc}_{\mathrm{uni}}$	A^2	B^2	C^2
2^{-11}	2048	6.696e−1	—	3.213e−3	—	1.446e4	7.644e3	1.924e−10
2^{-12}	4096	2.807e−1	1.254	1.062e−3	1.597	1.671e4	1.156e4	9.759e−13
2^{-13}	8192	6.974e−2	2.009	3.036e−4	1.807	1.480e4	1.684e4	8.836e−13
2^{-14}	16384	1.058e−2	2.720	8.545e−5	1.829	1.057e4	2.371e4	8.563e−13
2^{-15}	32768	1.311e−3	3.013	2.694e−5	1.666	7.707e3	3.220e4	8.498e−13
2^{-16}	65536	2.706e−4	2.276	8.859e−6	1.604	6.026e3	4.182e4	8.484e−13

TABLE 4. Performance of the midpoint method for the harmonic map heat flow in the presence of singularities.

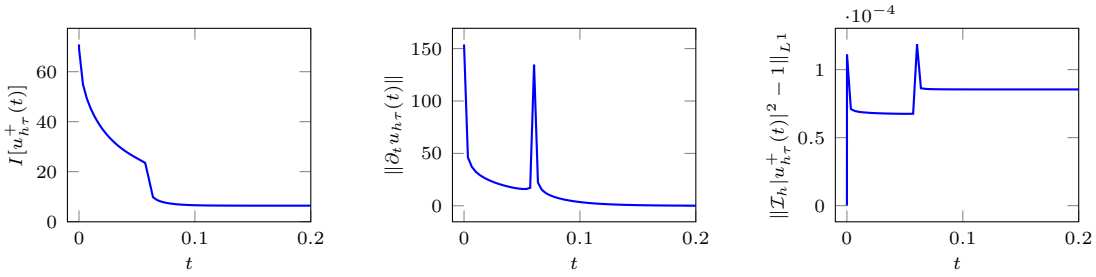

FIGURE 3. Evolution in $[0, 1/5]$ of the energy (left), the L^2-norm of the update (middle), and the constraint violation L^1-error (right) for the approximations generated by the midpoint method ($\tau = 2^{-14}$).

Looking at the results in Table 4, we observe the convergence of the constraint violation errors, but the rate is only superlinear. In particular, the convergence of $\delta_{\mathrm{uni}}[u_h^N]$ is not of second order, which is in agreement with the unboundedness of B^2, for which we observe a moderate grow. In Fig. 3, for $\tau = 2^{-14}$, we show the evolution in $[0, 1/5]$ of the energy $I[u_{h\tau}^+(t)]$, of the L^2-norm of $\|\partial_t u_{h\tau}(t)\|$, and of the constraint violation error $\|\mathcal{I}_h|u_{h\tau}^+(t)|^2 - 1\|_{L^1}$ (note that we omit the results for $t \in (1/5, 1]$ because the curves are nearly constant, as the evolution has already reached the stationary state). Here, $u_{h\tau}(t)$ (resp., $u_{h\tau}^+(t)$) denotes the globally continuous and piecewise affine interpolant (resp., the forward piecewise constant interpolant) of the sequence of snapshots $(u_h^n)_{n\geqslant 0}$. Looking at the evolution of the energy, we see an abrupt decay at $t \approx 0.06$, which is when the singularity disappears. In this phase, the dynamics is faster, as the spike in the plot of $\|\partial_t u_{h\tau}(t)\|$ reveals, which leads to a local growth of $\|\mathcal{I}_h|u_{h\tau}^+(t)|^2 - 1\|_{L^1}$.

4.2. **Variable step size.** In this section, we present two numerical experiments to showcase the performance of the midpoint method with variable step size.

4.2.1. *Prescribed variable step size.* Consider the projection-free linearly implicit midpoint method with variable step size τ_n, i.e., the iteration defined by (25) with $\theta = \mu = 1/2$ for $n \geqslant 2$ (initialized by one step of the implicit Euler method with step size τ_1 for $n = 1$). From the analysis of Section 3, we obtain that the iterates generated by the scheme satisfy the discrete energy law

$$\frac{1}{2}\|\nabla u^m\|^2 + \sum_{n=1}^{m} \tau_n \|d_t u^n\|_\star^2 + \frac{\tau_1^2}{2}\|\nabla d_t u^1\|^2 = \frac{1}{2}\|\nabla u^0\|^2 \tag{34}$$

and the upper bound of the constraint violation error

$$\begin{aligned} \||u^m|^2 - 1\|_{L^1} \leqslant \frac{1}{2}\left(\tau_1^2\|d_t u^1\|^2 + \tau_m^2\|d_t u^m\|^2 + \sum_{n=2}^{m} \tau_n^4 \|d_t^2 u^n\|^2\right) \\ + \frac{1}{2}\sum_{n=1}^{m-1} \tau_n^2 |1 - s_{n+1}^2| \|d_t u^n\|^2; \end{aligned} \tag{35}$$

see (26) and (30), respectively. We now aim to exploit the flexibility given by the variable step size to accelerate the convergence to stationary configurations.

First of all, motivated by the heuristic fact that the step size should increase as the iteration evolves toward convergence, we aim to obtain a nondecreasing sequence of step sizes, i.e., we impose that $\tau_n \leqslant \tau_{n+1}$ or, equivalently, $s_{n+1} \geqslant 1$.

Consider now the right-hand side of (35), which consists of two terms. Up to the generalization to variable step sizes, the first term is the same term that is present in the corresponding estimate for the method with constant step size. This term decays quadratically with respect to the step size if a discrete regularity condition is satisfied. The second term arises when the step size used in the method is not constant. Motivated by the similarity of this term to the second term on the left-hand side of (34), and observing that the latter is uniformly bounded, we aim to define τ_{n+1} in such a way that the step size powers in the two terms on the right-hand side of (35) are balanced, which is true if $|1 - s_{n+1}^2| = s_{n+1}^2 - 1 = c\tau_n$ for some $c > 0$. Manipulating this identity, we obtain the step size update

$$\tau_{n+1} = \tau_n \sqrt{1 + c\tau_n}. \tag{36}$$

To numerically validate this choice, we repeat the experiments of Sections 4.1.1 and 4.1.2 for the linearly implicit midpoint method with variable step size. We consider the initial step size $\tau_1 = 2^{-m}$ for $m = 6, \dots, 10$ for the H^1-gradient flow (resp., $m = 10, \dots, 16$ for the L^2-gradient flow) and update it during the iteration using the aforementioned formula with $c = 1$, i.e., $\tau_{n+1} = \tau_n\sqrt{1 + \tau_n}$.

The results of the simulation are displayed in Table 5, where we collect the same outputs considered before, plus the value $\tau_{N_{\text{stop}}}$ of the step size at the final iteration.

Looking at the results obtained for the H^1-gradient flow and comparing them with those obtained for constant step size (see the third table in Table 1), we see that the quality of the results improves significantly and the method with variable step size clearly overcomes the one using a constant step size. Indeed, for the same computational cost, i.e., if the number of iterations is approximately the same, the constraint violation error observed for the method with variable step size is much smaller: e.g., for about 2000 iterations (obtained for $\tau = 2^{-7}$ in the case of constant step size), the constraint violation error measured in the L^1-norm is of the order of 10^{-6}; for the same number of iterations, the method with variable step size yields an error of the order of 10^{-8}. Looking at the other

midpoint method with $\tau_{n+1} = \tau_n\sqrt{1+\tau_n}$ (H^1-gradient flow)								
τ_1	N_{stop}	$\tau_{N_{\text{stop}}}$	$\delta_\infty[u_h^{N_{\text{stop}}}]$	$\delta_{\text{uni}}[u_h^{N_{\text{stop}}}]$	$\delta_{\text{ener}}[u_h^{N_{\text{stop}}}]$	A^2	B^2	C^2
2^{-6}	139	183.5	1.775e−5	5.605e−6	3.010e−4	1.435e−3	1.242e−1	1.247e−18
2^{-7}	266	9.413	4.710e−6	1.488e−6	2.882e−4	7.250e−4	1.261e−1	2.319e−16
2^{-8}	522	4.042	1.216e−6	3.843e−7	2.847e−4	3.644e−4	1.271e−1	3.591e−16
2^{-9}	1035	3.938	3.091e−7	9.774e−8	2.838e−4	1.827e−4	1.276e−1	2.816e−17
2^{-10}	2059	2.158	7.795e−8	2.465e−8	2.836e−4	9.147e−5	1.278e−1	1.969e−16

midpoint method with $\tau_{n+1} = \tau_n\sqrt{1+\tau_n}$ (L^2-gradient flow)								
τ_1	N_{stop}	$\tau_{N_{\text{stop}}}$	$\delta_\infty[u_h^{N_{\text{stop}}}]$	$\delta_{\text{uni}}[u_h^{N_{\text{stop}}}]$	$\delta_{\text{ener}}[u_h^{N_{\text{stop}}}]$	A^2	B^2	C^2
2^{-10}	319	0.001 200	5.503e−3	2.485e−3	8.865e−3	7.148e2	4.441e3	9.574e−13
2^{-11}	637	5.780e−4	2.011e−3	7.780e−4	2.433e−3	5.831e2	5.857e3	9.616e−13
2^{-12}	1272	2.890e−4	7.102e−4	2.267e−4	4.894e−4	4.261e2	7.058e3	9.926e−13
2^{-13}	2543	1.445e−4	2.370e−4	6.251e−5	7.227e−5	2.819e2	7.954e3	9.971e−13
2^{-14}	5086	7.225e−5	7.465e−5	1.659e−5	2.276e−4	1.721e2	8.552e3	9.934e−13
2^{-15}	10170	3.612e−5	2.290e−5	4.295e−6	2.691e−4	9.928e1	8.918e3	9.977e−13
2^{-16}	20339	1.806e−5	6.902e−6	1.095e−6	2.798e−4	5.518e1	9.128e3	9.983e−13

TABLE 5. Midpoint method with prescribed variable step size.

quantities, we see that the lack of convergence of the energy values is the same for both variants of the method and that the discrete regularity condition seems to hold.

For the L^2-gradient flow (compare the second table in Table 5 with the third table in Table 2), we see that the difference in the performance of the midpoint method in the case of constant and variable step sizes is negligible. We conclude that the prescribed step size update rule is very effective for energy minimization in the case of the H^1-gradient flow, but not very impactful for the L^2-gradient flow.

4.2.2. *Adaptive step size control.* In this subsection, we endow the linearly implicit midpoint method with a simple adaptive mechanism, which allows to adjust the step size without assuming any knowledge on the specific problem data.

Specifically, for all $n \geqslant 2$, after the computation of the update $d_t u_h^n$ via (25) and the definition of the new approximation $u_h^n = u_h^{n-1} + \tau_n d_t u_h^n$, we adjust the step size τ_{n+1} for the next iteration according to the following rule: Given $0 < \tau_{\min} < \tau_{\max}$, if $\|d_t u_h^n\| > \|d_t u_h^{n-1}\|$, then we reduce the step size for the next iteration as $\tau_{n+1} = \max\{\tau_{\min}, \tau_n\sqrt{1-\tau_n/\tau_{\max}}\}$; otherwise, if $\|d_t u_h^n\| \leqslant \|d_t u_h^{n-1}\|$, then we enlarge the step size as $\tau_{n+1} = \min\{\tau_{\max}, \tau_n\sqrt{1+\tau_n/\tau_{\max}}\}$. The approach reduces the step size whenever the gradient flow dynamics accelerates, conversely the step size increases if the dynamics slows down. The specific formula for the adjustment comes from the discussion in Section 4.2.1 (cf. (36)), where we choose $c = 1/\tau_{\max}$ to guarantee that the step size is always positive.

We test the approach using the setups of Section 4.1.4 (harmonic map heat flow with singular solutions). We consider the initial step size $\tau_1 = 2^{-m}$ for $m = 11, \dots, 16$. Moreover, we set $\tau_{\min} = 2^{-18}$ and $\tau_{\max} = 1$.

adaptive midpoint method						
τ_0	N	$\delta_\infty[u_h^N]$	$\delta_{\text{uni}}[u_h^N]$	A^2	B^2	C^2
2^{-11}	1721	7.053e−1	3.478e−3	1.435e4	7.644e3	7.489e−5
2^{-12}	3250	2.855e−1	1.075e−3	1.666e4	1.156e4	9.792e−13
2^{-13}	6497	7.343e−2	3.104e−4	1.494e4	1.684e4	8.837e−13
2^{-14}	12991	1.130e−2	8.661e−5	1.071e4	2.371e4	8.571e−13
2^{-15}	25981	1.403e−3	2.707e−5	7.786e3	3.220e4	8.496e−13
2^{-16}	51960	2.706e−4	8.873e−6	6.066e3	4.182e4	8.482e−13

TABLE 6. Performance of the midpoint method with adaptively adjusted step size for the harmonic map heat flow in the presence of singularities.

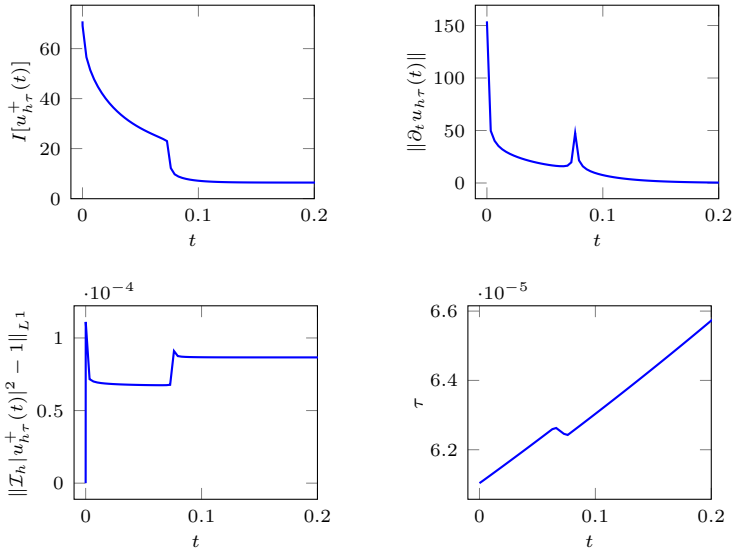

FIGURE 4. Evolution in $[0, 1/5]$ of the energy (top-left), the L^2-norm of the update (top-right), the constraint violation L^1-error (bottom-left), and the step size (bottom-right) for the approximations generated by the midpoint method with adaptively adjusted step size ($\tau_1 = 2^{-14}$).

Comparing the results in Table 6 and Fig. 4 with those obtained for constant step size (see Table 4), we see that the number of iterations N needed by the adaptive method to simulate the gradient flow dynamics in the interval of interest (a measure of the overall computational cost of the simulation) is reduced by 20% despite achieving approximately the same accuracy in the realization of the unit-length constraint. In Fig. 4 (bottom-right), we see that the reduction of the computational cost is obtained by increasing the step size throughout the entire evolution, except for $t \in (0.06, 0.08)$, where the faster dynamics (cf. the plots in Fig. 4 (top)) requires a more accurate time discretization.

REFERENCES

[1] C. Abert, G. Hrkac, M. Page, D. Praetorius, M. Ruggeri, and D. Suess. Spin-polarized transport in ferromagnetic multilayers: an unconditionally convergent FEM integrator. *Comput. Math. Appl.*, 68(6):639–654, 2014. doi:10.1016/j.camwa.2014.07.010.

[2] G. Akrivis, S. Bartels, and C. Palus. Quadratic constraint consistency in the projection-free approximation of harmonic maps and bending isometries. *Math. Comp.*, 94(355):2251–2269, 2025. doi:10.1090/mcom/4035.

[3] G. Akrivis, M. Chen, J. Han, F. Yu, and Z. Zhang. The variable two-step BDF method for parabolic equations. *BIT Numer. Math.*, 64(1):Paper No. 14, 21, 2024. doi:10.1007/s10543-024-01007-y.

[4] G. Akrivis, M. Feischl, B. Kovács, and C. Lubich. Higher-order linearly implicit full discretization of the Landau-Lifshitz-Gilbert equation. *Math. Comp.*, 90(329):995–1038, 2021. doi:10.1090/mcom/3597.

[5] F. Alouges. A new algorithm for computing liquid crystal stable configurations: the harmonic mapping case. *SIAM J. Numer. Anal.*, 34(5):1708–1726, 1997. doi:10.1137/S0036142994264249.

[6] F. Alouges. A new finite element scheme for Landau–Lifchitz equations. *Discrete Contin. Dyn. Syst. Ser. S*, 1(2):187–196, 2008. doi:10.3934/dcdss.2008.1.187.

[7] F. Alouges, E. Kritsikis, J. Steiner, and J.-C. Toussaint. A convergent and precise finite element scheme for Landau-Lifschitz-Gilbert equation. *Numer. Math.*, 128(3):407–430, 2014. doi:10.1007/s00211-014-0615-3.

[8] F. Alouges and A. Soyeur. On global weak solutions for Landau-Lifshitz equations: existence and nonuniqueness. *Nonlinear Anal.*, 18(11):1071–1084, 1992. doi:10.1016/0362-546X(92)90196-L.

[9] R. An, H. Gao, and W. Sun. Optimal error analysis of Euler and Crank-Nicolson projection finite difference schemes for Landau-Lifshitz equation. *SIAM J. Numer. Anal.*, 59(3):1639–1662, 2021. doi:10.1137/20M1335431.

[10] J. W. Barrett, S. Bartels, X. Feng, and A. Prohl. A convergent and constraint-preserving finite element method for the p-harmonic flow into spheres. *SIAM J. Numer. Anal.*, 45(3):905–927, 2007. doi:10.1137/050639429.

[11] S. Bartels. Stability and convergence of finite-element approximation schemes for harmonic maps. *SIAM J. Numer. Anal.*, 43(1):220–238, 2005. doi:10.1137/040606594.

[12] S. Bartels. *Numerical methods for nonlinear partial differential equations*, volume 47 of *Springer Series in Computational Mathematics*. Springer, 2015. doi:10.1007/978-3-319-13797-1.

[13] S. Bartels. Projection-free approximation of geometrically constrained partial differential equations. *Math. Comp.*, 85(299):1033–1049, 2016. doi:10.1090/mcom/3008.

[14] S. Bartels, J. Ko, and A. Prohl. Numerical analysis of an explicit approximation scheme for the Landau–Lifshitz–Gilbert equation. *Math. Comp.*, 77(262):773–788, 2008. doi:10.1090/S0025-5718-07-02079-0.

[15] S. Bartels, B. Kovács, and Z. Wang. Error analysis for the numerical approximation of the harmonic map heat flow with nodal constraints. *IMA J. Numer. Anal.*, 44(2):633–653, 2024. doi:10.1093/imanum/drad037.

[16] S. Bartels, C. Lubich, and A. Prohl. Convergent discretization of heat and wave map flows to spheres using approximate discrete Lagrange multipliers. *Math. Comp.*, 78(267):1269–1292, 2009. doi:10.1090/S0025-5718-09-02221-2.

[17] S. Bartels, C. Palus, and Z. Wang. Quasi-optimal error estimates for the finite element approximation of stable harmonic maps with nodal constraints. *SIAM J. Numer. Anal.*, 61(4):1819–1834, 2023. doi:10.1137/22M1524497.

[18] R. Becker, X. Feng, and A. Prohl. Finite element approximations of the Ericksen-Leslie model for nematic liquid crystal flow. *SIAM J. Numer. Anal.*, 46(4):1704–1731, 2008. doi:10.1137/07068254X.

[19] K.-C. Chang, W. Y. Ding, and R. Ye. Finite-time blow-up of the heat flow of harmonic maps from surfaces. *J. Differential Geom.*, 36(2):507–515, 1992. doi:10.1142/9789813220881_0023.

[20] J. Chen, C. Wang, and C. Xie. Convergence analysis of a second-order semi-implicit projection method for Landau–Lifshitz equation. *Appl. Numer. Math.*, 168:55–74, 2021. doi:10.1016/j.apnum.2021.05.027.

[21] G. Di Fratta, C.-M. Pfeiler, D. Praetorius, M. Ruggeri, and B. Stiftner. Linear second-order IMEX-type integrator for the (eddy current) Landau-Lifshitz-Gilbert equation. *IMA J. Numer. Anal.*, 40(4):2802–2838, 2020. doi:10.1093/imanum/drz046.

[22] P. Grohs, H. Hardering, and O. Sander. Optimal a priori discretization error bounds for geodesic finite elements. *Found. Comput. Math.*, 15(6):1357–1411, 2015. doi:10.1007/s10208-014-9230-z.

[23] G. Hrkac, C.-M. Pfeiler, D. Praetorius, M. Ruggeri, A. Segatti, and B. Stiftner. Convergent tangent plane integrators for the simulation of chiral magnetic skyrmion dynamics. *Adv. Comput. Math.*, 45(3):1329–1368, 2019. doi:10.1007/s10444-019-09667-z.

[24] Q. Hu, X.-C. Tai, and R. Winther. A saddle point approach to the computation of harmonic maps. *SIAM J. Numer. Anal.*, 47(2):1500–1523, 2009. doi:10.1137/060675575.

[25] B. Kovács, B. Li, and C. Lubich. A convergent evolving finite element algorithm for mean curvature flow of closed surfaces. *Numer. Math.*, 143(4):797–853, 2019. doi:10.1007/s00211-019-01074-2.

[26] B. Kovács, B. Li, and C. Lubich. A convergent algorithm for forced mean curvature flow driven by diffusion on the surface. *Interfaces Free Bound.*, 22(4):443–464, 2020. doi:10.4171/ifb/446.

[27] J. Kraus, C.-M. Pfeiler, D. Praetorius, M. Ruggeri, and B. Stiftner. Iterative solution and preconditioning for the tangent plane scheme in computational micromagnetics. *J. Comput. Phys.*, 398:108866, 2019. doi:10.1016/j.jcp.2019.108866.

[28] R. H. Nochetto, M. Ruggeri, and S. Yang. Gamma-convergent projection-free finite element methods for nematic liquid crystals: the Ericksen model. *SIAM J. Numer. Anal.*, 60(2):856–887, 2022. doi:10.1137/21M1407495.

[29] A. Ramage and E. C. Gartland, Jr. A preconditioned nullspace method for liquid crystal director modeling. *SIAM J. Sci. Comput.*, 35(1):B226–B247, 2013. doi:10.1137/120870219.

[30] J. Schöberl. NETGEN An advancing front 2D/3D-mesh generator based on abstract rules. *Comput. Vis. Sci.*, 1(1):41–52, 1997. doi:10.1007/s007910050004.

Department of Computer Science and Engineering, University of Ioannina, 451 10 Ioannina, Greece & Institute of Applied and Computational Mathematics, FORTH, 700 13 Heraklion, Greece
Email address: akrivis@cse.uoi.gr

Department of Applied Mathematics, University of Freiburg, 79104 Freiburg i. Br., Germany
Email address: bartels@mathematik.uni-freiburg.de

Department of Mathematics, University of Bologna, 40126 Bologna, Italy
Email address: m.ruggeri@unibo.it

School of Science, Harbin Institute of Technology, Shenzhen 518055, China
Email address: wangjilu@hit.edu.cn